

## Article

# Improvement of the Tribological Properties of Alumina Coatings by Zirconia Addition

Jacob Shiby Mathew <sup>1</sup>, Liutauras Marcinauskas <sup>1,2,\*</sup>, Mitjan Kalin <sup>3</sup>, Romualdas Kėželis <sup>2</sup>, Žydrūnas Kavaliauskas <sup>2,4</sup>, Giedrius Gecevičius <sup>4</sup> and Vytautas Čapas <sup>4</sup>

<sup>1</sup> Department of Physics, Kaunas University of Technology, Studentų Str. 50, LT-51368 Kaunas, Lithuania; jacob.mathew@ktu.lt

<sup>2</sup> Plasma Processing Laboratory, Lithuanian Energy Institute, Breslaujos Str. 3, LT-44403 Kaunas, Lithuania; romualdas.kezelis@lei.lt (R.K.); zydrunas.kavaliauskas@lei.lt (Ž.K.)

<sup>3</sup> Laboratory for Tribology and Interface Nanotechnology, Faculty of Mechanical Engineering, University of Ljubljana, Bogišičeva 8, 1000 Ljubljana, Slovenia; mitjan.kalin@tint.fs.uni-lj.si

<sup>4</sup> Kaunas University of Applied Sciences, Pramonės Ave. 20, LT-50468 Kaunas, Lithuania; giedrius.gecevicus@go.kauko.lt (G.G.); vytautas.capas@go.kauko.lt (V.Č.)

\* Correspondence: liutauras.marcinauskas@lei.lt; Tel.: +370-6151-0490

**Abstract:** Al<sub>2</sub>O<sub>3</sub> and Al<sub>2</sub>O<sub>3</sub>-ZrO<sub>2</sub> coatings were deposited on stainless steel using atmospheric plasma spraying. The influence of arc current and zirconia addition on the surface morphology of the coating, phase composition and tribological properties under dry sliding conditions were investigated. The addition of zirconia reduced the surface roughness of the coatings. The X-ray diffraction measurements indicated that the Al<sub>2</sub>O<sub>3</sub> coatings were composed of β-Al<sub>2</sub>O<sub>3</sub>, α-Al<sub>2</sub>O<sub>3</sub>, and γ-Al<sub>2</sub>O<sub>3</sub> phases. The addition of zirconia led to the formation of tetragonal and monoclinic phases of zirconia in the as-sprayed coatings. The friction coefficients of Al<sub>2</sub>O<sub>3</sub> and Al<sub>2</sub>O<sub>3</sub>-ZrO<sub>2</sub> coatings were similar and varied in the range of 0.72–0.75. The specific wear rates of the as-sprayed coatings were reduced with the increase of arc current. It was obtained that the wear rates of the Al<sub>2</sub>O<sub>3</sub>-ZrO<sub>2</sub> coatings were at least three times lower compared to Al<sub>2</sub>O<sub>3</sub> coatings.

**Keywords:** plasma spraying; air-hydrogen plasma; alumina-zirconia; tribology; friction coefficient



**Citation:** Mathew, J.S.; Marcinauskas, L.; Kalin, M.; Kėželis, R.; Kavaliauskas, Ž.; Gecevičius, G.; Čapas, V. Improvement of the Tribological Properties of Alumina Coatings by Zirconia Addition. *Coatings* **2021**, *11*, 991. <https://doi.org/10.3390/coatings11080991>

Academic Editors: Francesco Di Quarto and Devis Bellucci

Received: 15 June 2021

Accepted: 11 August 2021

Published: 20 August 2021

**Publisher's Note:** MDPI stays neutral with regard to jurisdictional claims in published maps and institutional affiliations.



**Copyright:** © 2021 by the authors. Licensee MDPI, Basel, Switzerland. This article is an open access article distributed under the terms and conditions of the Creative Commons Attribution (CC BY) license (<https://creativecommons.org/licenses/by/4.0/>).

## 1. Introduction

Aluminum oxide coatings have received wide attention because of their good mechanical and tribological properties, high resistance to thermal degradation and corrosion and a low electrical conductivity. These excellent properties allow alumina to be used in various fields like wear or corrosion protection of metal surfaces [1–6]. However, despite their high hardness, the alumina coatings are brittle and have relatively high friction coefficients under dry sliding conditions. In order to improve the toughness, brittleness, thermal or tribological properties of alumina coatings, various additives such as ZrO<sub>2</sub> [7–10], TiO<sub>2</sub> [7,11], graphite [12], and graphene nanoplatelets [13] are used.

Atmospheric plasma spraying is one of the most popular thermal spray processes used for the deposition of alumina and alumina composite coatings. It was demonstrated that the final properties of alumina coatings are strongly related to the phase composition as well as the amount of additives [2–5,8–10,12,14,15]. The variation of the spraying parameters (power, distance, substrate temperature, feedstock powder injection place) and feedstock powders characteristics (size, shape, composition etc.) strongly affects the phase composition and properties of the sprayed coatings [2–5,8–10,14,16]. It was demonstrated that the presence of γ-Al<sub>2</sub>O<sub>3</sub> phase enhanced the thermal and electrical properties. Meanwhile, the α-Al<sub>2</sub>O<sub>3</sub> phase could increase the hardness and dielectric properties of the alumina or alumina composite coatings [1,2,15]. Deng et al. [1] demonstrated that the friction coefficient and wear rate strongly depend on the counterpart body type used. The coefficient of

friction (CoF) value and specific wear rate of Al<sub>2</sub>O<sub>3</sub> was ~0.62 and  $2.85 \times 10^{-4}$  mm<sup>3</sup>/Nm, when Al<sub>2</sub>O<sub>3</sub> ball was used.

One of the most common additives used to improve the thermal, corrosion, tribological and mechanical properties of alumina coatings is zirconium oxide [5–9,14,15,17–25]. It was demonstrated that the yttria partially stabilized zirconia (YSZ)-Al<sub>2</sub>O<sub>3</sub> composite coatings can be used as common thermal barrier coatings for jet engines, gas turbines or diesel engines [5,23,24]. Those coatings allow one to reduce the metal surface temperatures, impart high thermal resistance and enhance durability of coated components [5,23–25]. Another important field of application of Al<sub>2</sub>O<sub>3</sub>-ZrO<sub>2</sub> coatings is to protect metallic surfaces from wear and reduce the friction coefficient under dry sliding conditions [6–9,17–22]. It was verified that an Al<sub>2</sub>O<sub>3</sub> coating reinforced by ZrO<sub>2</sub> demonstrated an average friction coefficient of about 0.92 under a 5 N load and a test duration of 10–30 min [7]. The microhardness was reduced but the toughness was improved with the increase in ZrO<sub>2</sub> content in the Al<sub>2</sub>O<sub>3</sub> coatings [8]. Liang et al. [9] demonstrated that the friction coefficients of ZrO<sub>2</sub>-15 wt.% Al<sub>2</sub>O<sub>3</sub> coatings were higher than for ZrO<sub>2</sub>-30 wt.% Al<sub>2</sub>O<sub>3</sub> and varied in the range of 0.2–0.75 depending on the loads and sliding velocities used, while the wear rates of ZrO<sub>2</sub>-Al<sub>2</sub>O<sub>3</sub> coatings changed from  $15 \times 10^{-6}$  up to  $100 \times 10^{-6}$  mm<sup>3</sup>/Nm [9]. Kim et al. [17] found that the incorporation of CaF<sub>2</sub> into Al<sub>2</sub>O<sub>3</sub>-15 wt.% ZrO<sub>2</sub> coatings reduced the microhardness and friction coefficients but increased the wear rates. It should also be noted that the friction coefficients of Al<sub>2</sub>O<sub>3</sub>-15 wt.% ZrO<sub>2</sub> coating varied in the range of 0.4 to 0.9 depending on the tribological test parameters. Zhao et al. [14] obtained that the friction coefficients and specific wear rates for Al<sub>2</sub>O<sub>3</sub>-15 wt.% ZrO<sub>2</sub> coatings were in ranges of 0.40–0.45 and  $(5–18) \times 10^{-5}$  mm<sup>3</sup>/Nm, respectively. Yu et al. [18] indicated that the mechanical properties and wear resistance of Al<sub>2</sub>O<sub>3</sub>-20 wt.% ZrO<sub>2</sub> coatings were improved by laser melting. Zhang et al. [19] demonstrated that the friction coefficient of Al<sub>2</sub>O<sub>3</sub>-40 wt.% ZrO<sub>2</sub> coating was 0.74, while with the addition of 3 wt.% Y<sub>2</sub>O<sub>3</sub> into the coating, the friction coefficient was reduced by ~22%. It was observed that the friction coefficient of Al<sub>2</sub>O<sub>3</sub>-ZrO<sub>2</sub> coating was higher by 40%, while the wear rate was about 15% lower compared to Al<sub>2</sub>O<sub>3</sub> coating sprayed using identical parameters [16]. Dejang et al. [20] obtained that the addition of ZrO<sub>2</sub> increased the  $\gamma$ -Al<sub>2</sub>O<sub>3</sub> phase fraction and improved the fracture toughness, reduced the friction coefficient and wear rate of coatings. Tingaud et al. [22] observed that the friction coefficient was slightly higher, but the wear rate was up to nine times lower when ZrO<sub>2</sub> is introduced into alumina coatings.

These studies demonstrated that the tribological properties of the alumina-zirconia coatings strongly depend on the used load values, counterbody properties, initial composition and type of employed Al<sub>2</sub>O<sub>3</sub>-ZrO<sub>2</sub> feedstock powders, as well as on the spraying process conditions [6–9,17–22]. However, it is hard to properly compare the obtained tribological properties of Al<sub>2</sub>O<sub>3</sub> and Al<sub>2</sub>O<sub>3</sub>-ZrO<sub>2</sub> coatings as the different studies used various tribological testing techniques from pin-on-disk to ball-on-disk, and various types of counterpart balls (from Si<sub>3</sub>N<sub>4</sub> to Al<sub>2</sub>O<sub>3</sub> to steels) with various ball diameters (Table 1) [1,2,14,16–20,22]. Also, the applied loads used for the tribological test of the coatings ranged from a few Newtons up to 60 N or even higher values, and various sliding velocities were applied [1,2,9,14,22]. It should be highlighted that most of the alumina and alumina-zirconia coatings are sprayed using argon or argon-hydrogen gas [1–3,8,9,14,15,22]. Meanwhile, the use of oxygen, nitrogen, or air as the main gases to form plasma for the deposition of alumina or alumina-zirconia coatings is less studied [12,26]. One of the aforementioned gas type drawbacks is that it increases the likelihood of surface oxidation or could cause the formation of undesirable compounds such as nitrides, which is not always desirable. However, the application of the air as the primary gas could be cost-effective as the gas consumption in plasma spraying is quite high. The information relating to the formation of alumina-zirconia coatings by an air-hydrogen plasma and the tribological behavior of such coatings is quite limited in the scientific literature. The main aim of this research was to investigate the influence of arc current and zirconia addition on the surface

morphology, phase composition and tribological properties of Al<sub>2</sub>O<sub>3</sub> coatings sprayed using an air-hydrogen gas mixture by atmospheric plasma spraying.

**Table 1.** Tribological test parameters and properties of various coatings.

Authors	Coating	Tribological Test	Counterpart	Loads, N	Sliding Velocity m/s	CoF	Wear Rate, mm <sup>3</sup> /Nm
B. Liang et al. [9]	Al <sub>2</sub> O <sub>3</sub> -ZrO <sub>2</sub>	Ball-on-disk	100C6 steel ball, 6 mm	2, 5	0.2, 0.5, 0.8, 1.1	0.15–0.70	(15–100) × 10 <sup>-6</sup>
R. Younes et al. [7]	Al <sub>2</sub> O <sub>3</sub> -ZrO <sub>2</sub>	Pin-on-disk	Al <sub>2</sub> O <sub>3</sub> -TiO <sub>2</sub>	5, 10, 15, 30	0.5	0.2–0.92	(0.5–1.3) mg/m
X. Zhao et al. [14]	Al <sub>2</sub> O <sub>3</sub> -ZrO <sub>2</sub>	Ball-on-disk	Steel ball, 10 mm	20–60	0.02	0.40–0.45	(4.5–18) × 10 <sup>-5</sup>
Wang et al. [15]	Al <sub>2</sub> O <sub>3</sub> -ZrO <sub>2</sub> , Al <sub>2</sub> O <sub>3</sub> -ZrO <sub>2</sub> - CeO <sub>2</sub>	Ball-on-disk	Si <sub>3</sub> N <sub>4</sub> ball, 4 mm	30	400 r/min	0.74, 0.61	0.864 × 10 <sup>-3</sup> , 0.592 × 10 <sup>-3</sup>
G. Darut et al. [16]	Al <sub>2</sub> O <sub>3</sub> , Al <sub>2</sub> O <sub>3</sub> -YSZ	Ball-on-disk	Al <sub>2</sub> O <sub>3</sub> ball, 6 mm	2	0.1	0.30–0.50, 0.50–0.60	(86–990) × 10 <sup>-6</sup> , 73 × 10 <sup>-6</sup>
S. Kim et al. [17]	Al <sub>2</sub> O <sub>3</sub> -ZrO <sub>2</sub>	Ball-on-plate	Al <sub>2</sub> O <sub>3</sub> ball, 12.7 mm	5–20	-	0.4–0.90	(2–20) × 10 <sup>-6</sup>
J. Yu et al. [18]	Al <sub>2</sub> O <sub>3</sub> -ZrO <sub>2</sub>	Ball-on-disk	Si <sub>3</sub> N <sub>4</sub> ball	-	-	-	-
X. Zhang et al. [19]	Al <sub>2</sub> O <sub>3</sub> -ZrO <sub>2</sub> , Al <sub>2</sub> O <sub>3</sub> -ZrO <sub>2</sub> - Y <sub>2</sub> O <sub>3</sub>	Ball-on-disk	Si <sub>3</sub> N <sub>4</sub> ball, 4 mm	30	4.985	0.74, 0.58	0.864 × 10 <sup>-3</sup> , 0.661 × 10 <sup>-3</sup>
N. Dejang et al. [20]	Al <sub>2</sub> O <sub>3</sub> , Al <sub>2</sub> O <sub>3</sub> -ZrO <sub>2</sub>	Pin-on-disk	WC/Co pin ball, 6.3 mm	0.98	79.5 rpm	0.62, 0.13–0.18	4.4 × 10 <sup>-4</sup> , (0.18–1.26) × 10 <sup>-4</sup>
O. Tingaud et al. [22]	Al <sub>2</sub> O <sub>3</sub> , Al <sub>2</sub> O <sub>3</sub> -YSZ	Pin-on-disk	Al <sub>2</sub> O <sub>3</sub> ball, 6 mm	2	0.1	0.38, 0.42, 0.39, 0.44	(3.7–5.2) × 10 <sup>-6</sup> (0.4–0.7) × 10 <sup>-6</sup>

## 2. Materials and Methods

The substrates used for the deposition of coatings were made from AISI 304L steel (40 mm × 10 mm × 1.5 mm). The plasma torch used for the deposition of coatings was designed and built at the Lithuanian Energy Institute (Kaunas, Lithuania) [12]. The coatings were sprayed using an air and hydrogen gas mixture. A total air flow rate of 4.72 and 4.70 g/s was used for the plasma jet formation and feedstock powder injection when Al<sub>2</sub>O<sub>3</sub> and Al<sub>2</sub>O<sub>3</sub>-10 wt.% ZrO<sub>2</sub> coatings were deposited, respectively. An air flow rate of 0.60 g/s was used for the feedstock powder injection. Additionally, hydrogen gas with the flow rate of ~0.1 g/s was used. The hydrogen gas was injected inside the reactor nozzle. The addition of the hydrogen was used in order to enhance the plasma temperature and increase the melting degree of feedstock powders. Al<sub>2</sub>O<sub>3</sub> (non-regular shape, size range from 63 to 140 μm, 98.5% purity) and ZrO<sub>2</sub>-8%Y<sub>2</sub>O<sub>3</sub> (type ZRO-113/114, 99% purity, spherical shape, purchased from PRAXAIR Surface Technologies, Indianapolis, IN, USA) powders were used to spray the coatings. The mixture of alumina and zirconia powders of Al<sub>2</sub>O<sub>3</sub>-10 wt.% ZrO<sub>2</sub> was prepared. The feedstock powders were mechanically mixed for 24 h and dried before the deposition. The steel samples were placed on water cooled holder in the distance of 70 mm from the plasma torch nozzle. The plasma torch arc currents during the experiments were 180 and 220 A. The plasma torch was moving forward and backward during the spraying. The deposition duration was ~40 s. The detailed plasma spraying parameters are given in Table 2. More detailed information on the experimental setup and the methodology for calculations of average plasma velocity and temperature at the nozzle outlet are found in [12].

**Table 2.** Deposition conditions of the coatings.

Parameter	Al <sub>2</sub> O <sub>3</sub>	Al <sub>2</sub> O <sub>3</sub>	Al <sub>2</sub> O <sub>3</sub> -ZrO <sub>2</sub>	Al <sub>2</sub> O <sub>3</sub> -ZrO <sub>2</sub>
Current, A	180	220	180	220
Voltage, V	205	195	200	190
Power, kW	36.9	42.9	36.0	41.8
Velocity, m/s	1350 ± 20	1385 ± 20	1330 ± 20	1370 ± 20
Temperature at exit, K	3400 ± 50	3485 ± 50	3420 ± 50	3490 ± 50

A S-3400N scanning electron microscope (SEM, Hitachi, Tokyo, Japan) and a portable SurfTest SJ-210 Series surface roughness tester (Version 2.00 with standard ISO 1997 Mitutoyo, Kawasaki, Japan) were used for the surface morphology and roughness analysis of the coatings, respectively. Linear roughness of the coatings was measured and the length of one profile measurement was 4 mm. Three samples of each type of coating type were measured and at least four measurements of each sample were done in order to calculate average linear roughness values. Error bars represent the standard deviation values. The energy dispersive X-ray spectroscopy (EDX) method (Bruker Quad 5040 spectrometer, AXS Microanalysis GmbH, Billerica, MA, USA) was used for determination of elemental composition of sprayed coatings. The EDX measurements were done for a surface area of ~1.15 mm<sup>2</sup> (magnification was 100×) at 5 different points using 15 kV acceleration voltage. The structure of the coatings was analyzed using X-ray diffraction (XRD) (Bruker D8 Discover, Billerica, MA, USA) with a standard Bragg-Brentano focusing geometry in a 5°–80° range using the CuKα ( $\lambda = 0.154059$  nm) radiation. A ball-on-flat configuration on a tribometer (UMT-2, CETR, Campbell, CA, USA) was used for measuring the tribological properties of prepared coatings and the initial steel substrate. A sliding velocity of 0.05 m/s for 50 min (distance 150 m) with a constant normal load of 0.8 N was used for the tests. The length of stroke in the tribological test was 5 mm. The tribological tests on the alumina coatings were done three times for two samples of each series. Meanwhile, two samples for each series of alumina-zirconia coatings were tested at two different surface areas. The mean friction coefficient was calculated using the last 10% of the data values [12]. All tribological tests were performed in dry-sliding conditions at 21 °C with a relative humidity RH = 20 ± 5%. As the counterpart a 10 mm diameter Al<sub>2</sub>O<sub>3</sub> ball (purity 99.5% and grade 10) was used. A 3D white-light optical interferometer (Counter GT-K0, Bruker, Billerica, MA, USA), with the use of the Vision64 software were used for the examination of the amount of coating removed during the tribological tests.

### 3. Results and Discussions

SEM images of the alumina and alumina-zirconia coatings deposited at various arc currents are given in Figure 1. It can be seen that for the aluminum oxide coatings, the amount of molten particles had increased, and the size of particles had slightly reduced at the higher torch power (Figure 1a–d). Spherical and irregular shaped particles of size from 1 to 20 µm could be found. The Al<sub>2</sub>O<sub>3</sub> coatings had some pores, voids and micro-cracks (Figure 1b,d). The surfaces of the Al<sub>2</sub>O<sub>3</sub>-ZrO<sub>2</sub> coatings are slightly more homogenous and smoother than the Al<sub>2</sub>O<sub>3</sub> coatings. The surface contains partially and fully molten particle zones, spheroidized particles, and also, some voids and pores could be observed (Figure 1f,h). The thickness of the alumina coatings was 30–40 µm. The thicknesses of the Al<sub>2</sub>O<sub>3</sub>-ZrO<sub>2</sub> coatings were up to 40 and ~70 µm prepared at 180 A and at 220 A, respectively. With increasing arc current, it could be seen that the melting degree of the particles had enhanced as the average plasma temperature had increased by ~70–85 K. It should be noted that the plasma jet temperature was higher than the melting points of alumina (~2320 K) and zirconia (~2950 K) feedstock powders [8]. With the enhancement in arc current from 180 to 220 A, globule-like formations could be perceived, and cauliflower-like structures could be ascertained (Figure 1h). The small amount of unmelted or semi-molten particle fragments obtained on the surface of the coatings prepared at the higher arc current is due

to the lower temperature in the peripheral region of the plasma jet and the different sizes of feedstock powders used [15].

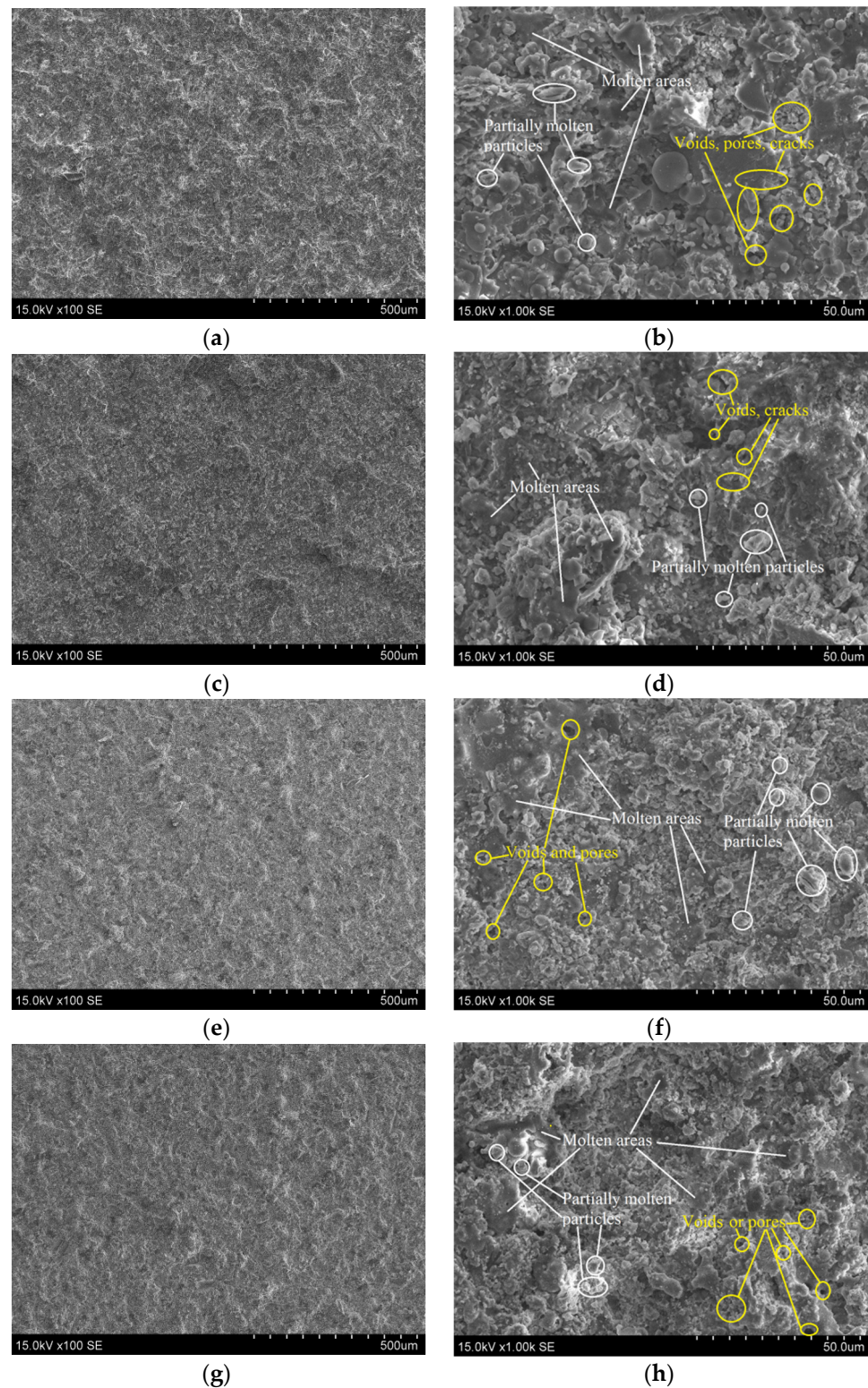


**Figure 1.** Surface morphology of (a–d)  $\text{Al}_2\text{O}_3$  and (e–h)  $\text{Al}_2\text{O}_3\text{-ZrO}_2$  coatings sprayed at (a,b,e,f) 180 and (c,d,g,h) 220 A.

The distribution of the oxygen, zirconium, aluminum, and yttrium on the surface of the  $\text{Al}_2\text{O}_3\text{-ZrO}_2$  coatings are presented in Figure 2. The images indicated that the

alumina and zirconia feedstock powders were homogeneously spread on the surface. The EDX measurements indicated that the major elements found in the alumina-zirconia coatings were aluminum (Figure 2e,i), oxygen (Figure 2c,g), zirconium (Figure 2d,h), yttrium (Figure 2f,j) alongside a low amount of impurities. The composition of oxygen was found to be marginally reduced from ~21.9 wt.% (~50.0 at.%) to 20.4 wt.% (~48.7 at.%) with the increase in arc current. Similarly, for aluminum, a slight reduction from 18.8 wt.% (~25.4 at.%) to ~16.2 wt.% (~24.4 at.%) was observed. Despite the addition of only 10 wt.% of  $ZrO_2$  powders into alumina, the content of zirconium was 52.7 wt.% (~21.6 at.%) and 56.2 wt.% (~23.5 at.%), respectively. The fraction of yttrium had slight increase from 4.97 wt.% (~2.1 at.%) to 5.61 wt.% (~2.4 at.%) with the increase in arc current.

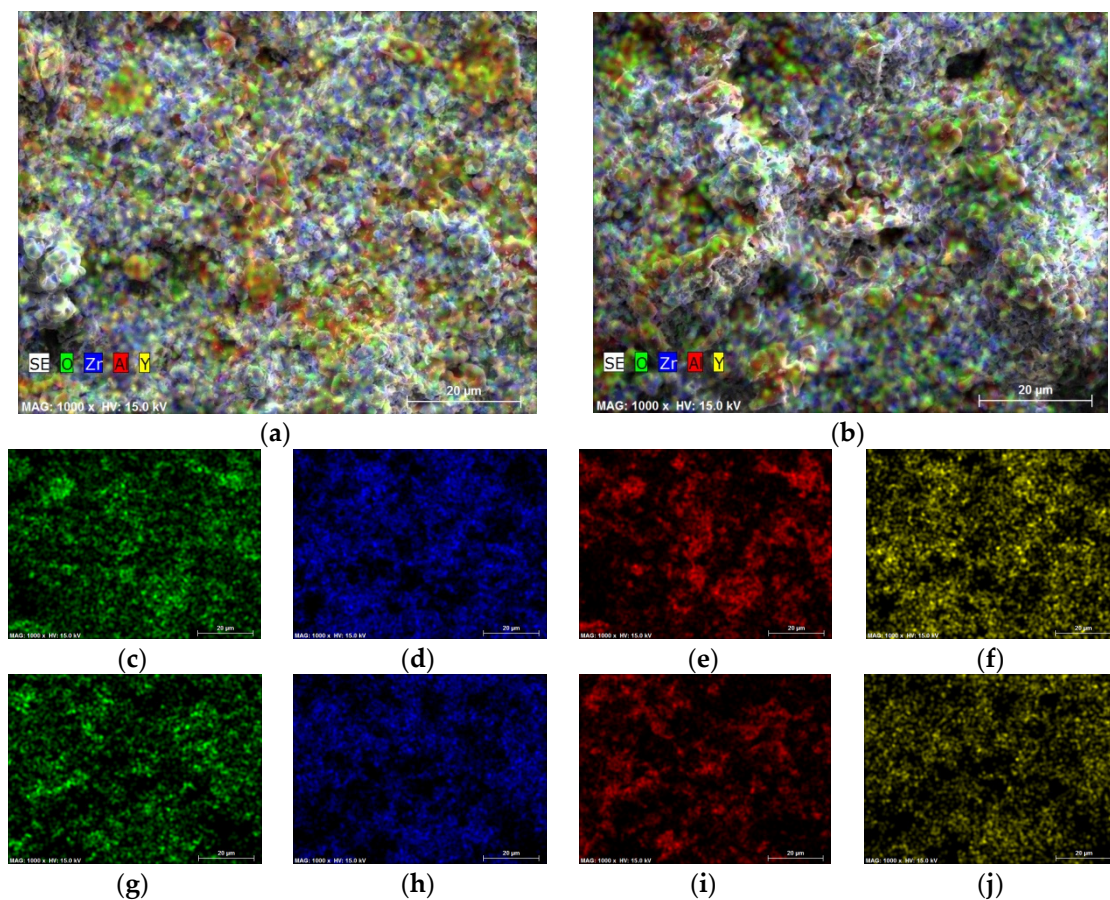


**Figure 2.** Surface micrographs and elemental maps of  $Al_2O_3$ - $ZrO_2$  coatings deposited at (a,c–f) 180 A and (b,g–j) 220 A, (c,g) oxygen, (d,h) zirconium, (e,i) aluminum and (f,j) yttrium.

The used  $Al_2O_3$  and  $ZrO_2$  feedstock powders were mixed mechanically. Thus, due to different size and shape of used  $Al_2O_3$  (non-regular shape) and  $ZrO_2$  (mainly spherical shape) powders and their densities, the flowability of powders would be different. Also, it could result into separation and segregation of the powders in the feeder. Thus, probably more of  $ZrO_2$  powders would be injected during the deposition. Also, some amount of alumina powders could be lost in plasma plume due to melting and vaporization of powders, as the  $Al_2O_3$  melting temperatures are lower than compared to  $ZrO_2$  powders. The elemental composition of  $Al_2O_3$  was aluminum and oxygen, with a low amount of impurities (Fe, Na) related to the nature of the employed feedstock powders, in addition to carbon due to absorption of the atmospheric gases. The weight percentage ratio of oxygen to aluminum (O/Al) slightly decreased from 1.00 to 0.97 with the enhancement of arc current for the alumina coatings.

The average surface roughness ( $R_a$ ) and the root-mean-square roughness ( $R_q$ ) of the  $\text{Al}_2\text{O}_3$  coating deposited at 180 A was  $\sim 3.79$  and  $4.69$   $\mu\text{m}$ , respectively (Figure 3). The surface roughness of the  $\text{Al}_2\text{O}_3$  coating increased to  $R_a = 4.56$   $\mu\text{m}$  and  $R_q = 5.58$   $\mu\text{m}$  with the increase of arc current. As regards the average surface roughness of alumina-zirconia coatings, the  $R_a$  increased from  $\sim 2.28$  to  $3.43$   $\mu\text{m}$ , with increase in arc current from 180 to 220 A, respectively. The  $R_q$  values had followed a similar trend with values at 180 and 220 A arc currents being  $3.04$  and  $4.35$   $\mu\text{m}$ . Thus, with the increase of the plasma jet temperature, the roughness of the coatings increased, while the addition of  $\text{ZrO}_2$  reduced the surface roughness. Usually, a higher melting degree of particle as plasma velocities increase results in a lower surface roughness of sprayed coatings [2,3,22]. The slightly higher surface roughness of the alumina-zirconia coating prepared at 220 A is due to the higher thickness value (as XRD (Figure 4) revealed only insignificant intensities of the steel substrate). The increase of roughness of  $\text{Al}_2\text{O}_3$  coating at higher arc current could be explained in such way: The  $\text{Al}_2\text{O}_3$  particles probably are only partly melted at 180 A and when it impacts the surface, partly melted particles split into smaller fragments and some of these fragments do not stick on the surface or are poorly adhered to it. As the temperature and velocity of the plasma are increased, the melting degree of the particles is enhanced, and a higher amount of particles would stick and be solidified on the surface. However, even at higher arc currents, the temperature required in order to fully melt the  $\text{Al}_2\text{O}_3$  particle was not reached. As a result, the surface roughness is slightly increased.

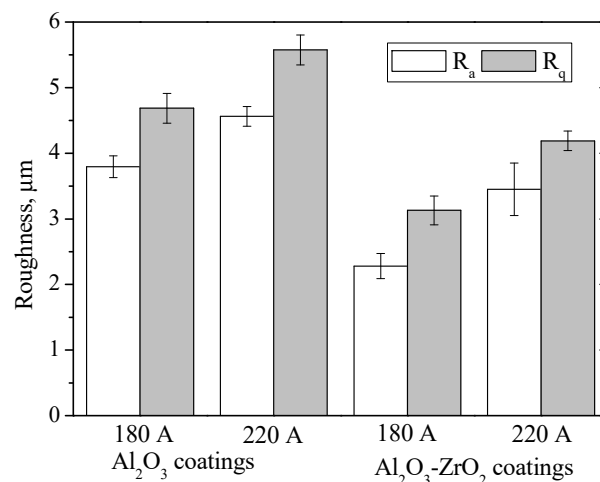


**Figure 3.** Surface roughness of the  $\text{Al}_2\text{O}_3$  and  $\text{Al}_2\text{O}_3\text{-ZrO}_2$  coatings.

The XRD patterns of the as-sprayed  $\text{Al}_2\text{O}_3$  and  $\text{Al}_2\text{O}_3\text{-ZrO}_2$  coatings are given in the Figure 4. The  $\text{Al}_2\text{O}_3$  coatings consisted of hexagonal  $\beta\text{-Al}_2\text{O}_3$ , rhombohedral  $\alpha\text{-Al}_2\text{O}_3$  and cubic  $\gamma\text{-Al}_2\text{O}_3$  phases. It was obtained that the beta- $\text{Al}_2\text{O}_3$  is the dominant phase. The peaks obtained at  $\sim 7.8^\circ$ ,  $\sim 15.7^\circ$  and  $\sim 33.2^\circ$  are assigned to sodium aluminum oxide (card No. 32–1033) with the  $\beta\text{-Al}_2\text{O}_3$  (002), (004) and (107) orientations, respectively [12]. The diffraction peaks found at  $\sim 25.7^\circ$ ,  $\sim 35.2^\circ$ ,  $\sim 37.8^\circ$ ,  $\sim 43.4^\circ$ ,  $\sim 52.6^\circ$  and  $\sim 57.6^\circ$  are related to  $\alpha\text{-Al}_2\text{O}_3$  phase of (012), (104), (110), (113), (024) and (116) orientations, respectively [3,12–15]. It should be noted that the initial alumina powders consisted of  $\alpha\text{-Al}_2\text{O}_3$  phase and sodium aluminum oxide ( $\text{NaAl}_{11}\text{O}_{17}$ ) (beta phase), and the intensities of  $\alpha\text{-Al}_2\text{O}_3$  peaks were dominant [27]. Meanwhile, the low intensity peaks at  $45.9^\circ$  and  $66.9^\circ$  are related to existence of  $\gamma$ -alumina phases in the coatings (Figure 4) [3,15]. It should be noted that the peaks at  $43.7^\circ$ ,  $50.7^\circ$  and  $74.6^\circ$  are attributed to the steel substrate [12]. The increase in arc current slightly changed the intensities of the alumina phase peaks. The relative intensities of the dominant peaks were taken, and different phase ratios were calculated. It was obtained that the  $\beta\text{-Al}_2\text{O}_3/\gamma\text{-Al}_2\text{O}_3$  ratio was slightly reduced from 6.0 to 5.9 with the increase in arc current. The  $\alpha\text{-Al}_2\text{O}_3/\gamma\text{-Al}_2\text{O}_3$  ratio decreased from 2.0 to 1.6, while  $\beta\text{-Al}_2\text{O}_3/\alpha\text{-Al}_2\text{O}_3$  ratio increased from 3.0 to 3.6 with the increase in arc current.

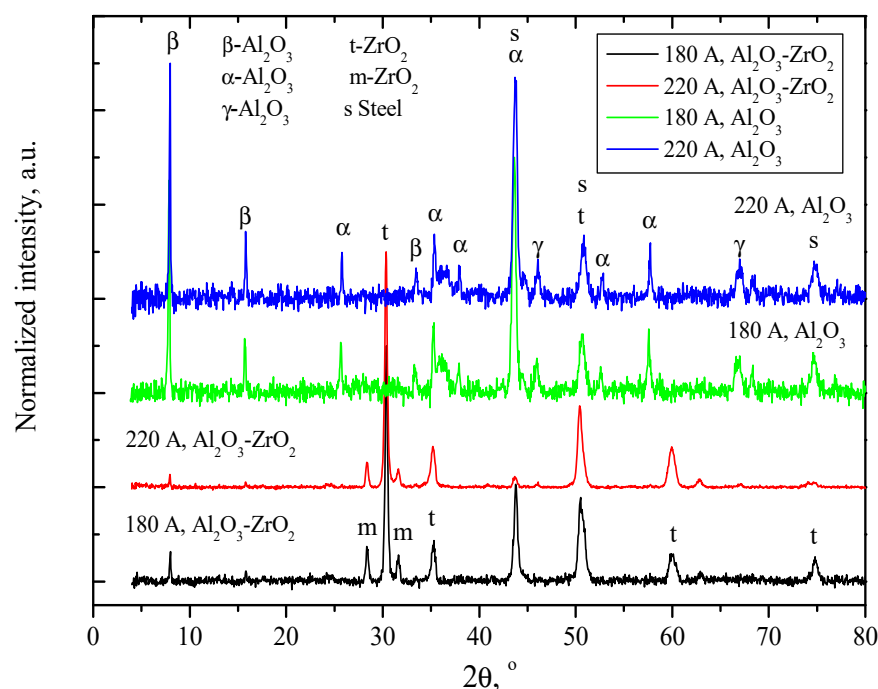


Figure 4. XRD patterns of the of  $\text{Al}_2\text{O}_3$  and  $\text{Al}_2\text{O}_3\text{-ZrO}_2$  coatings.

With the addition of zirconium oxide into the feedstock powders (Figure 4), the intensity of the alumina peaks in the XRD patterns of the  $\text{Al}_2\text{O}_3\text{-ZrO}_2$  coatings was drastically reduced. The dominant peaks were attributed to the tetragonal ( $t\text{-ZrO}_2$ ) and monoclinic phase ( $m\text{-ZrO}_2$ ) of zirconia [14,15,20,28]. The XRD patterns of the coatings had not showed the cubic phase of zirconia. The peaks found at  $2\theta = 30.2^\circ$  (101),  $35.3^\circ$  (110),  $50.5^\circ$  (200),  $59.96^\circ$  (211) are assigned to the  $t\text{-ZrO}_2$  phase [28]. Meanwhile the lower intensity peaks at  $\sim 28.4^\circ$  (111) and  $\sim 31.6^\circ$  ( $-111$ ) are attributed to the monoclinic  $\text{ZrO}_2$  phase [26,28]. The ratio of the highest peaks corresponding to  $t\text{-ZrO}_2$  ( $\sim 30.2^\circ$ ) and  $\alpha\text{-Al}_2\text{O}_3$  ( $\sim 35.2^\circ$ ) was hard to determine as  $\alpha\text{-Al}_2\text{O}_3$  peak overlapped with  $t\text{-ZrO}_2$  peak and was very weak. The increase in arc current also slightly enhanced the intensity of the  $\gamma\text{-Al}_2\text{O}_3$  peaks. The intensity ratio of  $t\text{-ZrO}_2/m\text{-ZrO}_2$  peaks were 6.7 and 9.5 for the coatings prepared at 180 and 220 A, respectively. While the  $t\text{-ZrO}_2/m\text{-ZrO}_2$  ratio was  $\sim 3.8$  in the feedstock powders. The  $m\text{-ZrO}_2$  phase fraction in total  $\text{ZrO}_2$  content was calculated using following equation [28]:

$$C_m = \frac{0.82(I_{m-111} + I_{m111})}{0.82(I_{m-111} + I_{m111}) + I_{t101}} \quad (1)$$

where  $C_m$  is the content of  $m\text{-ZrO}_2$  phase,  $I$  is the intensity of diffraction peak, subscript monoclinic (m) and tetragonal (t) the phase type.

The results indicated that the increase in arc current reduced the monoclinic phase content from  $\sim 17.6\%$  to  $13.2\%$ . It should be noted that the  $m\text{-ZrO}_2$  phase fraction in the YSZ feedstock powders was  $\sim 27.1\%$ . The reduction of the monoclinic phase in the coatings indicates the phase transformation during particle flight and solidification on the surface [19,26]. Also, the increase of the plasma jet temperature enhances the melting degrees of feedstock particles and leads to higher phase transformation values. With the increase in arc current from 180 to 220 A, the plasma temperature increases from 3400 to 3485 K and therefore, more  $\text{Al}_2\text{O}_3$  feedstock particles are fully melted, or the fraction of the molten state would be higher. Thus, this resulted in the slight increase of the beta- $\text{Al}_2\text{O}_3$  and gamma- $\text{Al}_2\text{O}_3$  phase fraction in the  $\text{Al}_2\text{O}_3$  coatings. It was demonstrated that with the increase of plasma arc current (plasma jet temperature) the content of the  $\alpha\text{-Al}_2\text{O}_3$  phase is reduced due to the higher degree of melting of the particles [1,3]. Tingaud et al. [22] found that the sprayed alumina and alumina-zirconia coatings mainly consisted of  $\alpha\text{-Al}_2\text{O}_3$

phase and only a minor fraction of  $\gamma$ - $\text{Al}_2\text{O}_3$  phase. The intensities of  $\alpha$ - $\text{Al}_2\text{O}_3$  peaks in our coatings is also higher compared to  $\gamma$ - $\text{Al}_2\text{O}_3$  (Figure 4). Usually, the  $\gamma$ - $\text{Al}_2\text{O}_3$  phase dominates in the as-sprayed  $\text{Al}_2\text{O}_3$  or  $\text{Al}_2\text{O}_3$  composite coatings [1,2,14,15]. Several reasons could be attributed to explain such obtained results. Firstly, the cooling rate of molten or partly molten particles on the surface is insufficient. That is, the high heat flux delivered by the plasma flow to the surface of the coating keeps the particles in the liquid state for the longer time and delays the solidification of lamellae. As a result, the gamma phase can recrystallize back into the alpha phase [2,15,26,29]. The second factor is that a partial heat treatment takes place during the deposition of the coatings. The surface of the coating is locally heated by the plasma torch as it moves over the substrate. Thus, the locally heated regions composing of the metastable gamma phase can partially re-transform into the stable alpha phase [2,22]. The third reason is associated to the fact that the coating contains unmelted or partially melted particles identical to the initial feedstock, i.e., the alumina powder with the dominant alpha phase [22,26]. The final factor is that the partially melted alumina particles are represented by a liquid fringe (gamma phase) and a solid heart (alpha phase). The solid part acts like a germ and spreads into all the grains, which then have the alpha phase as resultant [22]. The surface morphology images of the coatings indicated that at higher arc currents, a more compact surface morphology with lower size particles was formed. So, a better contact between individual splats was formed and the cohesion would be higher [3,15]. It was demonstrated that the level of the micropore volume typically obtained at splat boundaries of the sprayed  $\text{Al}_2\text{O}_3$  coatings is reduced when the melting degree of the particles is enhanced [2,3].

The variation of the friction coefficient versus sliding time for the  $\text{Al}_2\text{O}_3$  and  $\text{Al}_2\text{O}_3$ - $\text{ZrO}_2$  coatings is presented in Figure 5. As the tribo-run progressed, the friction coefficients of all the coatings gradually increased with time, eventually reaching steady state values of  $\sim 0.65$ – $0.70$  after 300–500 s. The further increase in sliding time resulted in only a marginal increase in the friction coefficients of the coatings and at higher time ranges (more than 1000 s), it fluctuated within a small range (Figure 5). In the running-in stage, the friction coefficient is enhanced due to the increase in dry sliding contact area caused by the reduction in surface roughness of the coatings. When the high asperities are cut in the contact area, the friction coefficient become stable. Thus, it indicates the wear behavior of the coupled materials [2]. It should be noted that the friction coefficient curve versus time of the alumina coatings demonstrated slightly higher fluctuations compared to  $\text{Al}_2\text{O}_3$ - $\text{ZrO}_2$ . It was obtained that the larger surface roughness resulted in the higher fluctuation of the friction coefficient curve [1].

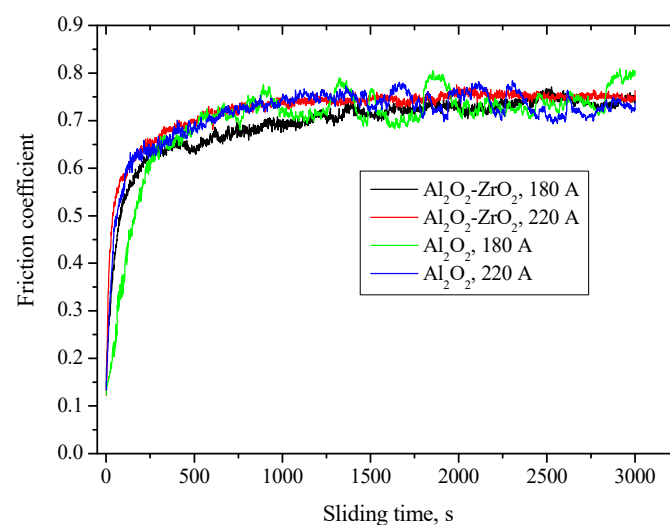


**Figure 5.** Friction coefficient curves of  $\text{Al}_2\text{O}_3$  and  $\text{Al}_2\text{O}_3$ - $\text{ZrO}_2$  coatings.

The coefficient of friction (CoF) was calculated when a steady state was reached and the last 10% of CoF values with the corresponding standard deviations were considered. The average steady state coefficients of friction of the sprayed coatings are given in Figure 6a. It should be noted that the average CoF values of the Al<sub>2</sub>O<sub>3</sub> coatings produced at 180 and 220 A were  $0.746 \pm 0.010$  and  $0.723 \pm 0.011$ , respectively. The addition of the ZrO<sub>2</sub> into the Al<sub>2</sub>O<sub>3</sub> feedstock powders only slightly changed the CoF values (Figure 6a). The alumina-zirconia coating prepared at 180 A demonstrated a CoF of  $\sim 0.735 \pm 0.015$ . With the increase in arc current, the average CoF value remained similar:  $0.736 \pm 0.042$ .

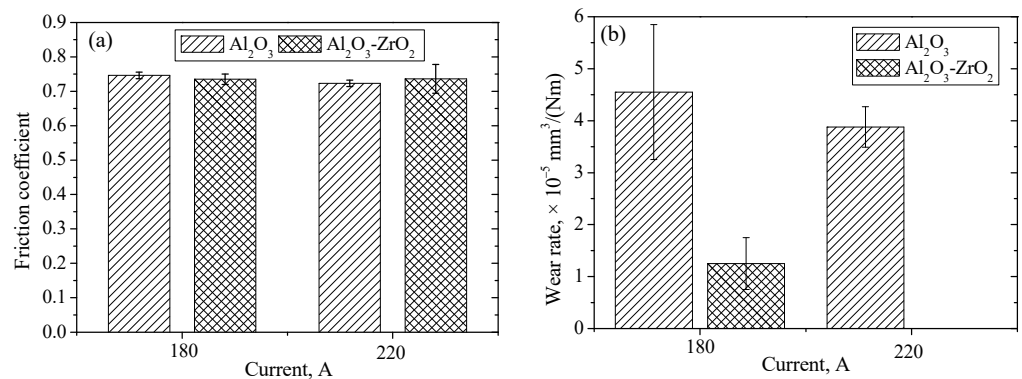


**Figure 6.** Friction coefficients (a) and specific wear rates (b) of Al<sub>2</sub>O<sub>3</sub> and Al<sub>2</sub>O<sub>3</sub>-ZrO<sub>2</sub> coatings.

The average wear rates of the alumina coatings deposited at 180 and 220 A were  $4.55 \times 10^{-5}$  and  $3.88 \times 10^{-5}$  mm<sup>3</sup>/Nm, respectively (Figure 6b). The addition of ZrO<sub>2</sub> reduced the specific wear rate down to  $1.25 \times 10^{-5}$  mm<sup>3</sup>/Nm for Al<sub>2</sub>O<sub>3</sub>-ZrO<sub>2</sub> deposited at 180 A. The normalized wear rate was found to be immeasurable, reasons owing to mere bulk-material transfer leading to plastic deformation, when the alumina-zirconia coating was deposited at 220 A. It should be noted that the wear rate of AISI 304 L steel was  $1.17 \times 10^{-4}$  mm<sup>3</sup>/Nm.

The tribological tests indicated that the friction coefficient and specific wear rate of Al<sub>2</sub>O<sub>3</sub> were slightly improved with the increase in arc current. Thus, the alumina particles would have reached higher temperatures in the plasma jet and when the particles impacted the substrate, a better contact between splats would have been obtained and the number of pores at the splat boundaries would have been reduced [3]. The Al<sub>2</sub>O<sub>3</sub>-ZrO<sub>2</sub> coatings had lower specific wear rates than Al<sub>2</sub>O<sub>3</sub>-coatings under the same formation conditions. These results indicate that the addition of zirconia improved the interfacial adhesion between individual splats and the mechanical properties, as a result, the wear resistance was enhanced [15]. Liang et al. [9] observed that the presence of more pores will cause a high stress concentration and lead to the formation of cracks, resulting in a low wear resistance.

As the plasma temperature increased, the deposited coatings would be denser and less porous, due to a higher particle melting degree and higher particle velocities and would thus, demonstrate better tribological properties [2,22,26]. Such a trend is related to the reduction of the poorly adhered particles embedded into the coating matrix at higher arc currents. As a result, the amount of the stacking defect density is reduced and higher cohesion values between lamellae is reached, thus the friction behavior of the coatings is improved. Meanwhile, the addition of zirconia led to the production of even denser, cohesive, more homogenous and smoother surface coatings. The specific wear rate of alumina-zirconia coatings is lower, despite the slightly higher or similar friction coefficient values compared to the alumina coatings. Thus, the addition of zirconia into the alumina matrix improved the wear resistance of the coatings. It should be noted that the friction coefficient increases as the contact area is higher [2,22]. The roughness of the alumina-zirconia coatings was  $\sim 25\%$  to  $40\%$  lower when compared to the alumina coatings. Thus, the contact area between the coating and counterbody part is larger, resulting in the

slightly higher friction coefficient values. Tingaud et al. [22] also demonstrated that the addition of zirconia enhanced the friction coefficient of the coatings up to 5%, but reduced the wear rate up to nine times, when compared to alumina. The authors' observation of improvement in the tribological properties is attributed to the higher cohesive values and a denser structure of the sprayed coatings [15,22].

The SEM images of the wear scar morphology of the coatings is presented in Figure 7. The worn surface tracks of the alumina coatings were non-homogenous. SEM images indicated that the width of tribological tracks were ~700–650 and ~600  $\mu\text{m}$  for the  $\text{Al}_2\text{O}_3$  coatings deposited at 180 and 220 A, respectively (Figure 7a,b). The surface of the coatings does not show formation of the micro-cracks or delamination of the splats. The wear track of the  $\text{Al}_2\text{O}_3\text{-ZrO}_2$  coating was ~500  $\mu\text{m}$  wide and was quite homogeneous in all length when 180 A was used (Figure 7c). There were some microcracks and wear grooves formed and peeled-off particles (wear debris) on the surface (Figure 7e) The wear track became slightly narrower, non-continuous and wear grooves are not pronounced for the coating deposited at 220 A (Figure 7d,f). SEM images demonstrated that the material was removed only from the top portion of the hills' region of the coating, and that the coating was insignificantly damaged after the tribological test. The wear debris found on the worn surface of all coatings indicate the abrasive wear mechanism [1].

Several authors indicated that the wear resistance of the  $\text{Al}_2\text{O}_3\text{-ZrO}_2$  [26],  $\text{Al}_2\text{O}_3\text{-ZrO}_2\text{-CeO}_2$  [15] and  $\text{Al}_2\text{O}_3\text{-ZrO}_2\text{-TiO}_2$  [29] coatings was improved due to enhancement of  $\alpha\text{-Al}_2\text{O}_3$  phase content and reduction of  $\gamma\text{-Al}_2\text{O}_3$  phase amount. The main reason for reduction of wear rate and in some cases, the friction coefficient of coatings, is that the  $\alpha\text{-Al}_2\text{O}_3$  phase has a higher hardness and elastic modulus, and also, fewer defects than  $\gamma\text{-Al}_2\text{O}_3$  [15,20,26,29]. The phase transformation of tetragonal to monoclinic  $\text{ZrO}_2$  phase was observed when comparing the XRD data of the feedstock powder and the  $\text{Al}_2\text{O}_3\text{-ZrO}_2$  coatings. It was observed that a significant volume expansion of approximately 3–5 vol.% occurs when the tetragonal phase is transformed to monoclinic [30]. As a result, a higher amount of micro-cracks and stress values between the steel substrate and the ceramic coating is observed [15,30]. Zhao et al. [14] obtained that the wear rate of  $\text{Al}_2\text{O}_3\text{-ZrO}_2$  coatings decreases (despite slightly higher friction coefficient values), due to the reduction of m- $\text{ZrO}_2$  phase and a better inter-splat bonding. The increase in the arc current from 180 to 220 A results in the higher plasma temperature and a better heat transfer to the feedstock particle. Thus, a higher inter-splat bonding between alumina and zirconia splats is obtained. Reduction of the intensities of  $\alpha\text{-Al}_2\text{O}_3$  and m- $\text{ZrO}_2$  phase peaks at higher arc currents is also attributed to the enhancement in the melted fraction of particles. Thus, the coatings sprayed at higher arc currents demonstrate an improved adhesion between the individual lamellae, are less porous, contain smaller sized pores and are denser. The reduction of pore sizes and semi-molten regions will suppress the pathways for the propagation of cracks and delamination of grains during the wear tests. The propagation of microcracks gradually peeled off the particles from the surface and the pulled-out (plowed) particles were crushed at the interaction zone between the coating and counterpart. Thus, the formed abrasive grains and wear debris could act as lubricants and slightly reduce the wear rate. However, the appearance of fluctuations on the friction curves of the  $\text{Al}_2\text{O}_3$  coatings (Figure 5), indicates that the particles act as abrasives and increase the wear rate of the coatings. Thus, the sprayed  $\text{Al}_2\text{O}_3$  coatings demonstrated slightly higher wear rates compared to the  $\text{Al}_2\text{O}_3\text{-ZrO}_2$  coatings (Figure 6b). Mehar et al. [29] indicated that at lower loads (15 N) plastic grooving and chipping were the dominant mechanisms of coatings wear. Wang et al. [15] showed that the CoF and wear rate of alumina-zirconia coatings were  $0.74 \times 10^{-3}$  and  $0.86 \times 10^{-3} \text{ mm}^3/\text{Nm}$  using 30 N, respectively. Several authors have indicated that the lower wear rate is associated with a better splat bonding adhesion, higher hardness, higher gamma phase content and lower porosity of alumina and alumina-zirconia coatings [2,14,15,22,29]. The wear grooves could be seen on the worn surface areas, the surface is much less removed in the alumina-zirconia coatings deposited

at 220 A (Figure 7d,f). This indicates that the lowest amount of material is removed due to the highest splat bonding interactions and the wear rate is reduced.

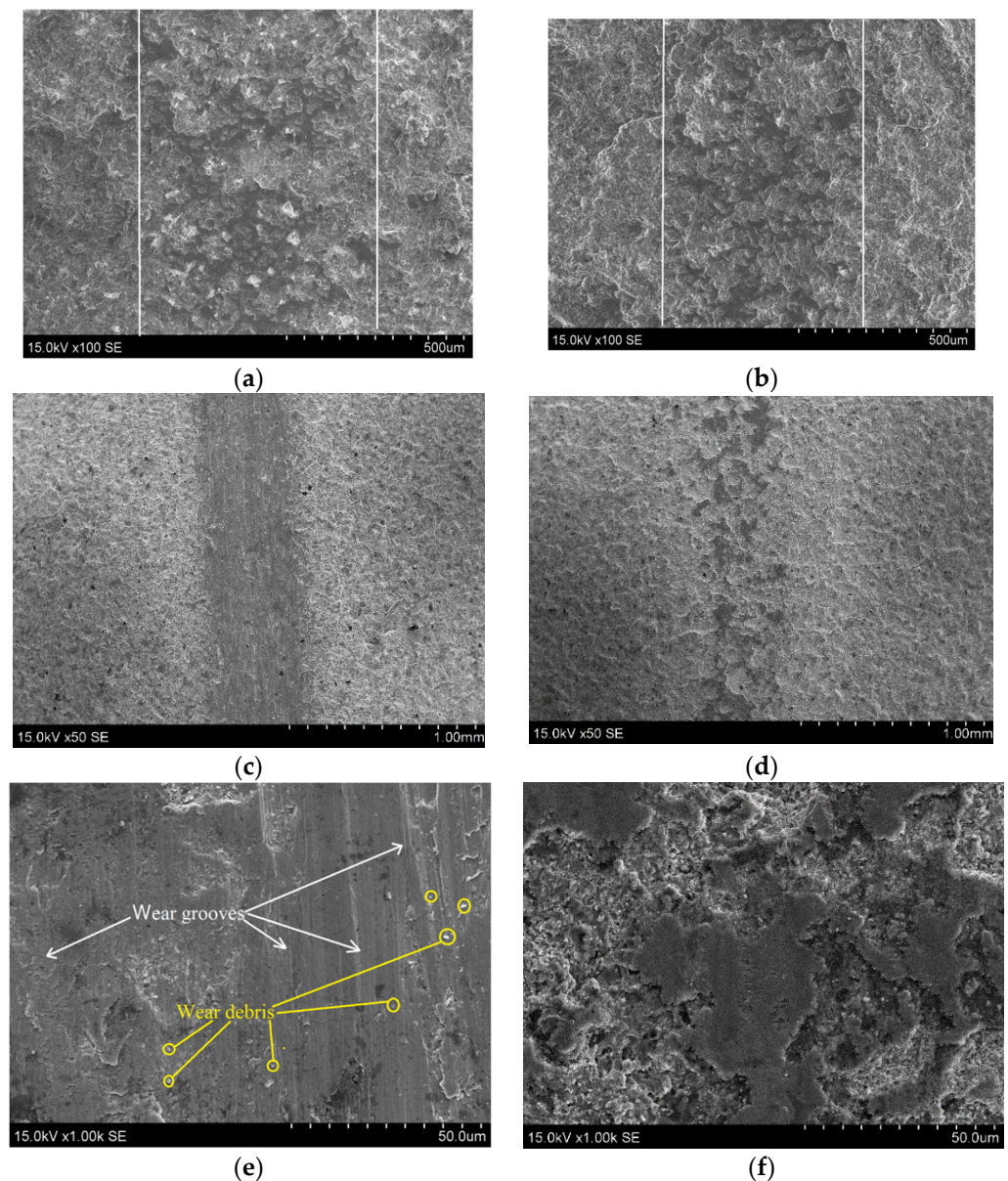


**Figure 7.** Wear scars images of (a,b)  $\text{Al}_2\text{O}_3$  and (c–f)  $\text{Al}_2\text{O}_3\text{-ZrO}_2$  coatings deposited at (a,c,e) 180 A and (b,d,f) 220 A.

#### 4. Conclusions

Alumina and alumina-zirconia coatings were formed by atmospheric plasma spraying using an air-hydrogen plasma. The increase in arc current increased the surface roughness of the  $\text{Al}_2\text{O}_3$  and  $\text{Al}_2\text{O}_3\text{-ZrO}_2$  coatings. However, with the addition of  $\text{ZrO}_2$ , the average surface roughness of the coatings was reduced up to 40%. The fraction of oxygen was reduced and an enhancement of Zr concentration was obtained at higher arc currents. The  $\text{Al}_2\text{O}_3$  coatings consisted of  $\beta\text{-Al}_2\text{O}_3$ ,  $\alpha\text{-Al}_2\text{O}_3$  and  $\gamma\text{-Al}_2\text{O}_3$  phases, and with the increase of arc current the  $\alpha\text{-Al}_2\text{O}_3$  phase content was slightly reduced. The dominant phases in the alumina-zirconia coatings were t- $\text{ZrO}_2$  and m- $\text{ZrO}_2$ . It was found that the increase in arc current from 180 to 220 A, reduced the monoclinic  $\text{ZrO}_2$  phase content from  $\sim 17.6\%$  to  $13.2\%$  in the  $\text{Al}_2\text{O}_3\text{-ZrO}_2$  coatings. The friction coefficient slightly decreased from 0.746 to 0.723, while the specific wear rate reduced from  $4.55 \times 10^{-5}$  to  $3.88 \times 10^{-5} \text{ mm}^3/(\text{Nm})$  for the

Al<sub>2</sub>O<sub>3</sub> coatings, with the increase in arc current. The addition of zirconia into the alumina feedstock powders had no effect on the friction coefficient values of the coatings. The wear rate of the Al<sub>2</sub>O<sub>3</sub>-ZrO<sub>2</sub> coating prepared at 180 A, was reduced ~3.6 times compared to Al<sub>2</sub>O<sub>3</sub>. The Al<sub>2</sub>O<sub>3</sub>-ZrO<sub>2</sub> coating deposited at 220 A demonstrated the highest wear resistance property and only an insignificant peeling of the hilltops on the surface of the wear scar zones was observed.

**Author Contributions:** Conceptualization, J.S.M., L.M., and Ž.K.; methodology, J.S.M., M.K., R.K., Ž.K., and V.Č.; software, J.S.M.; formal analysis, J.S.M., R.K., V.Č., and G.G.; investigation, J.S.M., L.M., M.K., and Ž.K.; data curation, J.S.M.; writing—original draft preparation, J.S.M., L.M., and Ž.K.; writing—review and editing, L.M. and J.S.M.; visualization, J.S.M. and G.G.; supervision, L.M. All authors have read and agreed to the published version of the manuscript.

**Funding:** This research received no external funding.

**Institutional Review Board Statement:** Not applicable.

**Informed Consent Statement:** Not applicable.

**Data Availability Statement:** Data sharing not applicable.

**Acknowledgments:** The authors thank S. Tučkutė from the Lithuanian Energy Institute for the performed SEM and EDX measurements.

**Conflicts of Interest:** The authors declare no conflict of interest.

## References

- Deng, W.; Li, S.; Hou, G.; Lia, X.; Zhao, X.; An, Y.; Zhou, H.; Chen, J. Comparative study on wear behaviour of plasma sprayed Al<sub>2</sub>O<sub>3</sub> coatings sliding against different counterparts. *Ceram. Int.* **2017**, *43*, 6976–6986. [CrossRef]
- Misra, V.; Chakravarthy, Y.; Khare, N.; Singh, K.; Ghoru, S. Strongly adherent Al<sub>2</sub>O<sub>3</sub> coating on SS 316L: Optimization of plasma spray parameters and investigation of unique wear resistance behaviour under air and nitrogen environment. *Ceram. Int.* **2020**, *46*, 8658–8668. [CrossRef]
- Wang, C.; Fan, L.; Fan, J.; Zhang, D.; Wang, H. Effect of spraying power on microstructure and properties of supersonic plasma sprayed Al<sub>2</sub>O<sub>3</sub> coating on porous Si<sub>3</sub>N<sub>4</sub> substrate. *J. Alloys Compd.* **2013**, *559*, 152–157. [CrossRef]
- An, Y.; Li, S.; Hou, G.; Zhao, X.; Zhou, H.; Chen, J. Mechanical and tribological properties of nano/micro composite alumina coatings fabricated by atmospheric plasma spraying. *Ceram. Int.* **2017**, *6*, 5319–5328. [CrossRef]
- Heimann, R.B. *Plasma Spray Coating Principles and Applications*; Wiley-VCH: Weinheim, Germany, 2008.
- Sathish, S.; Geetha, M. Comparative study on corrosion behavior of plasma sprayed Al<sub>2</sub>O<sub>3</sub>, ZrO<sub>2</sub>, Al<sub>2</sub>O<sub>3</sub>/ZrO<sub>2</sub> and ZrO<sub>2</sub>/Al<sub>2</sub>O<sub>3</sub> coatings. *Trans. Nonferr. Met. Soc. China* **2016**, *5*, 1336–1344. [CrossRef]
- Younes, R.; Bradai, M.; Sadeddine, A.; Mouadj, Y.; Bilek, A.; Benabbas, A. Effect of TiO<sub>2</sub> and ZrO<sub>2</sub> reinforcements on properties of Al<sub>2</sub>O<sub>3</sub> coatings fabricated by thermal flame spraying. *Trans. Nonferr. Met. Soc. China* **2016**, *26*, 1345–1352. [CrossRef]
- Chen, Y.; Yang, Y.; Chu, Z.; Chen, X.; Wang, L.; Liu, Z.; Dong, Y.; Yan, D.; Zhang, J.; Kang, Z. Microstructure and properties of Al<sub>2</sub>O<sub>3</sub>-ZrO<sub>2</sub> composite coatings prepared by air plasma spraying. *Appl. Surf. Sci.* **2018**, *431*, 93–100. [CrossRef]
- Liang, B.; Zhang, G.; Liao, H.; Coddet, C.; Ding, C. Friction and wear behaviour of ZrO<sub>2</sub>-Al<sub>2</sub>O<sub>3</sub> composite coatings deposited by air plasma spraying: Correlation with physical and mechanical properties. *Surf. Coat. Technol.* **2009**, *203*, 3235–3242. [CrossRef]
- Kiilakoski, J.; Musalek, R.; Luka, F.; Koivuluoto, H.; Vuoristo, P. Evaluating the toughness of APS and HVOF-sprayed Al<sub>2</sub>O<sub>3</sub>-ZrO<sub>2</sub>-coatings by in-situ- and macroscopic bending. *J. Eur. Ceram.* **2018**, *38*, 1908–1918. [CrossRef]
- Bannier, M.; Vicent, E.; Rayón, R.; Benavente, M.D.; Salvador, E.; Sánchez, E. Effect of TiO<sub>2</sub> addition on the microstructure and nanomechanical properties of Al<sub>2</sub>O<sub>3</sub> Suspension Plasma Sprayed coatings. *Appl. Surf. Sci.* **2014**, *316*, 141–146. [CrossRef]
- Marcinauskas, L.; Mathew, S.J.; Milieška, M.; Thanigachalam, B.; Kupec, A.; Česnavičius, R.; Kėželis, R.; Kalin, M. Microstructure and tribological properties of plasma sprayed alumina and alumina-graphite coatings. *Surf. Coat. Technol.* **2018**, *350*, 401–409. [CrossRef]
- Murray, J.W.; Ranceb, G.A.; Xua, F.; Hussain, T. Alumina-graphene nanocomposite coatings fabricated by suspension high velocity oxy-fuel thermal spraying for ultra-low-wear. *J. Eur. Ceram. Soc.* **2018**, *38*, 1819–1828. [CrossRef]
- Zhao, X.; An, Y.; Chen, J.; Zhou, H.; Yin, B. Properties of Al<sub>2</sub>O<sub>3</sub>-40 wt.% ZrO<sub>2</sub> composite coatings from ultra-fine feedstocks by atmospheric plasma spraying. *Wear* **2008**, *265*, 1642–1648. [CrossRef]
- Wang, Y.-w.; Wang, X.-l.; Wang, X.-y.; Yang, Y.; Zhang, C.; Sun, W.; Ma, Y.; Cui, Y.; Wang, L.; Dong, Y. Effect of CeO<sub>2</sub> on the Microstructure and Properties of Plasma-Sprayed Al<sub>2</sub>O<sub>3</sub>-ZrO<sub>2</sub> Ceramic Coatings. *J. Mater. Eng. Perform.* **2020**, *29*, 6390–6401. [CrossRef]
- Darut, G.; Ben-Ettouil, F.; Denoirjean, A.; Montavon, G.; Ageorges, H.; Fauchais, P. Dry sliding behavior of sub-micrometer-sized suspension plasma sprayed ceramic oxide coatings. *J. Therm. Spray Technol.* **2010**, *19*, 275–285. [CrossRef]

17. Kim, S.; Hannul, P.; Lee, W. Effects of the sliding conditions on the tribological behaviour of atmospheric plasma sprayed Al<sub>2</sub>O<sub>3</sub>-15 wt.% ZrO<sub>2</sub>-CaF<sub>2</sub> composite coating. *Surf. Coat. Technol.* **2012**, *210*, 27–134. [[CrossRef](#)]
18. Yu, J.; Wang, Y.; Zhou, F.; Wang, L.; Pan, Z. Laser remelting of plasma-sprayed nanostructured Al<sub>2</sub>O<sub>3</sub> 20 wt.% ZrO<sub>2</sub> coatings onto 316L stainless steel. *Appl. Surf. Sci.* **2018**, *431*, 112–121. [[CrossRef](#)]
19. Zhang, X.; Wang, Y.; Sun, W.; Yang, Y.; Zhang, C.; Ma, Y.; Cui, Y.; Zhao, C.; Wang, L.; Dong, Y.; et al. Microstructure and properties of Al<sub>2</sub>O<sub>3</sub>-ZrO<sub>2</sub>-Y<sub>2</sub>O<sub>3</sub> composite coatings prepared by plasma spraying. *J. Therm. Spray Technol.* **2020**, *29*, 967–978. [[CrossRef](#)]
20. Dejang, N.; Limpichaipanit, A.; Watcharapasorn, A.; Wirojanupatump, S.; Niranatlumpong, P.; Jiansirisomboon, S. Fabrication and properties of plasma-sprayed Al<sub>2</sub>O<sub>3</sub>/ZrO<sub>2</sub> composite coatings. *J. Therm. Spray Technol.* **2011**, *20*, 259–1268. [[CrossRef](#)]
21. Chen, D.; Jordan, E.; Gell, M. Microstructure of suspension plasma spray and air plasma spray Al<sub>2</sub>O<sub>3</sub>-ZrO<sub>2</sub> composite coatings. *J. Therm. Spray Technol.* **2009**, *22*, 421–426. [[CrossRef](#)]
22. Tingaud, O.; Bertrand, P.; Bertrand, G. Microstructure and tribological behavior of suspension plasma sprayed Al<sub>2</sub>O<sub>3</sub> and Al<sub>2</sub>O<sub>3</sub>-YSZ composite coatings. *Surf. Coat. Technol.* **2010**, *205*, 1004–1008. [[CrossRef](#)]
23. Jin, L.; Ni, L.; Yu, Q.; Rauf, A.; Zhou, C. Thermal cyclic life and failure mechanism of nanostructured 13 wt.%Al<sub>2</sub>O<sub>3</sub> doped YSZ coating prepared by atmospheric plasma spraying. *Ceram. Int.* **2012**, *38*, 2983–2989. [[CrossRef](#)]
24. Li, S.; Zhao, X.; Hou, G.; Deng, W.; An, Y.; Zhou, H.; Chen, J. Thermomechanical properties and thermal cycle resistance of plasma-sprayed mullite coating and mullite/zirconia composite coatings. *Ceram. Int.* **2016**, *42*, 17447–17455. [[CrossRef](#)]
25. Ramesh, M.; Marimuthu, K.; Karuppusamy, P.; Rajeshkumar, L. Microstructure and properties of YSZ-Al<sub>2</sub>O<sub>3</sub> functional ceramic thermal barrier coatings for military applications. *Bol. Soc. Esp. Ceram. Vidr.* **2021**, in press. [[CrossRef](#)]
26. Kiilakoski, J.; Puranen, J.; Heinonen, E.; Koivuluoto, H.; Vuoristo, P. Characterization of powder-presursor HVOF-Sprayed Al<sub>2</sub>O<sub>3</sub>-YSZ/ZrO<sub>2</sub> coatings. *J. Therm. Spray Technol.* **2019**, *28*, 98–107. [[CrossRef](#)]
27. Marcinauskas, L.; Milieška, M.; Kėželis, R. Effect of torch power on the microstructure of plasma sprayed Al<sub>2</sub>O<sub>3</sub> coatings. *Surf. Interface Anal.* **2016**, *6*, 552–555. [[CrossRef](#)]
28. Dong, H.; Yao, J.T.; Li, J.; Zhou, Y.; Li, Y.B. The sintering behavior of plasma-sprayed YSZ coating over the delamination crack in low temperature environment. *Ceram. Int.* **2018**, *44*, 3326–3332. [[CrossRef](#)]
29. Mehar, S.; Sapate, S.; Vashishtha, N.; Rathoda, A.; Bagdeb, P. Tribological performance of plasma sprayed Al<sub>2</sub>O<sub>3</sub>-TiO<sub>2</sub>-ZrO<sub>2</sub> ceramic coating. *Mater. Today.* **2021**, *45*, 4737–4741.
30. Bai, Y.; Han, Y.H.; Li, H.Q.; Xu, C.; Xu, Y.L.; Wang, Z.; Ding, C.H.; Yanf, J.F. High performance nanostructured ZrO<sub>2</sub> based thermal barrier coatings deposited by high efficiency supersonic plasma spraying. *Appl. Surf. Sci.* **2011**, *257*, 7210–7216. [[CrossRef](#)]